Multi-Functional Radar Waveform Generation Based on Optical Frequency-Time Stitching Method

Yamei Zhang, *Member, IEEE*, Ce Liu, Yu Zhang, Kunlin Shao, Cong Ma ⓘ, Lu Li ⓘ, Lijun Sun, Simin Li ⓘ, and Shilong Pan ⓘ, *Senior Member, IEEE, Senior Member, OSA*

Abstract—A photonic-assisted multi-functional radar waveform generator for single-chirped, counter-chirped, and dual-band linear frequency-modulated (LFM) microwave waveforms generation is proposed and experimentally demonstrated based on an optical frequency-stepped waveform (FSW) generator. The optical FSW generator is realized by an optical switch and an optical frequency shifting loop (OFSL). When an electrical rectangular LFM pulse is applied to the proposed signal generator, an optical frequency-stepped LFM signal would be generated. By carefully setting the time length and the bandwidth of the rectangular LFM pulse, we can achieve an optical linearly-chirped continuous wave. Optical frequency-time stitching is thus realized. Combining the optical linear-chirped signal with one or more optical wavelengths, and meticulously adjusting the value of the optical wavelengths, single-chirped, counter-chirped or dual-band LFM signals can be produced. An experiment is carried out. Single-chirped and counter-chirped LFM signals of 8–32 GHz over a time duration of 5 μs, and dual-band LFM signals of 8–16 GHz & 15–23 GHz and 8–20 GHz & 20–32 GHz are generated. The ambiguity functions of the generated signals are investigated.

Index Terms—Linear frequency modulation, microwave photonics, dual-chirp signal.

I. INTRODUCTION

LINEAR frequency-modulated (LFM) signal with a large time-bandwidth product (TBWP) is highly desired by modern radar systems to achieve simultaneously large detection range and high range resolution [1]–[3]. Conventionally, LFM signals are generated with pure electronic technologies by using a voltage-controlled oscillator (VCO) or a direct digital synthesizer (DDS), which can generate LFM signals with central frequency and instantaneous frequency limited to a few

gigahertz. However, the fast development of millimeter-wave technologies brings a tremendous challenge to the traditional electronic LFM signal generation methods. To remedy this, photonics-based LFM signal generation methods are proposed thanks to the innate characteristics of photonics [4]–[6] in terms of high frequency of 193 THz, broad bandwidth of several terahertz, low transmission loss of 0.2 dB/km, electromagnetic interference immunity etc. Plenty efforts have been paid out for generation of LFM signals in the photonic domain [7]–[18], with methods of spectral shaping and frequency to time mapping [7]–[10], photonic microwave phase modulation [11], externally optical injection of semiconductor laser [12]–[13], photonic microwave frequency multiplying [14]–[17], sweeping laser source [18]–[19], etc. However, the previously reported systems suffer from limited time duration, limited bandwidth, limited TBWP, or poor linearity. In addition, most of the previously reported systems can only generate LFM signals with single-chirped instantaneous frequency in a single frequency band, which is not suitable for multi-functional radar applications.

To deal with these issues, systems for the generation of LFM signals with multiple bands and (or) multiple chirped frequencies [20]–[24] are explored. In [20], a counter-chirped LFM signal generator based on a dual-parallel Mach-Zehnder modulator (DPMZM) is reported. By applying an RF signal and a baseband single-chirped LFM signal to the two sub-MZMs of the DPMZM, respectively, a counter-chirped LFM signal with its central frequency equal to the RF signal frequency and the bandwidth equal to the baseband-LFM bandwidth can be generated. However, the central frequency and the bandwidth of the produced counter-chirped LFM signal are confined by the electrical driven signals. In order to improve the central frequency and bandwidth, microwave photonic frequency multiplication is taken into consideration [21]–[23]. For example, dual-band LFM signal [21] and counter-chirped LFM signals [22], [23] with multiplied central frequencies and bandwidths are generated based on photonic microwave frequency multiplication in a polarization division multiplexing (PDM) DPMZM. However, due to the limited electro-optic effect of the electro-optic modulator, it is quite hard to realize photonic microwave frequency multiplying with a high multiplication factor (>6), indicating that a baseband signal generator with a high sampling rate is required for the generation of signals with high frequency and broad bandwidth. To deal with this problem, optical frequency-time stitching method is proposed [25]–[26]. The basic principle is to introduce multiple frequency shifts

and time delays to a basic LFM signal. After frequency-time stitching, a broadband LFM signal can be obtained. This method features large bandwidth, excellent linearity, and high flexibility. However, a programmable optical processor and two OFCs are required in [25] and optical switch and phase modulator arrays are required in [26], making the system bulky and costly.

Recently, we proposed and reported an optical frequency-stepped waveform (FSW) generator based on an optical frequency shifting loop (OFSL), which is characterized by simple configuration, large bandwidth and flexible reconfigurability [27]. The generator can produce an optical frequency-stepped signal with a large TBWP. In this paper, an LFM signal generator is realized by filling the frequency gaps of the optical frequency-stepped signal with an LFM signal. By incorporating the optical LFM signal generator with an optical wavelength generator, broadband and multifunctional waveforms can be generated. The optical wavelength generator could be a dual-arm MZM (DMZM), a DPMZM, a PDM-DMZM, a PDM-DPMZM or a combination of several modulators. The proposed system has the following advantages: (1) thanks to the employment of the OFSL, broadband LFM signal (potentially >50 GHz) can be generated without a high-sampling-rate waveform generator; (2) multi-functional LFM signals can be generated by meticulously adjusting the number and the wavelength of the output of the optical wavelength generator. If only one wavelength is generated by the optical wavelength generator, a single-chirped LFM signal can be obtained. If two wavelengths are produced by the optical wavelength generator, dual-band or counter-chirped LFM signals can be achieved. If more wavelengths are provided by the optical wavelength generator, more formats of LFM signals can be produced. An experiment is carried out. LFM signals with single-chirped and counter-chirped frequency of 8–32 GHz over a time duration of 5 μs are generated, and dual-band LFM signals with frequencies of 8–16 GHz & 15–23 GHz and 8–20 GHz & 20–32 GHz are obtained. The ambiguity functions of the generated signals are investigated, showing that the counter-chirped LFM signal has a good range-Doppler resolution.

II. PRINCIPLE

Figure 1 displays the schematic diagram of the proposed LFM signal generator, which is consisted of a laser diode (LD), an optical FSW generator, an optical wavelength generator, two optical couplers (OCs) and a photodetector (PD). A lightwave is first produced by the LD and is divided evenly into two paths via an OC (OC1). One of the paths is sent to the optical FSW generator that is realized by an optical switch (OS) and an OFSL. When an electrical rectangular pulse with a time width of τ and a repetition period of T_s is applied to the OS, and an RF signal with an angular frequency of ω_s is applied to the OFSL, the output of the OFSL could be written as [27],

$$E_{\mathrm{OFSL}}(t) = \sum_n \left\{ rect\left[\frac{t-nT_s-T_s/2}{T_s}\right] \right.$$
$$\left. \cdot \sum_{p=0}^{P-1} rect\left[\frac{t-p\tau-\tau/2-nT_s}{\tau}\right] \cos\left[(\omega_o + p\omega_s)\,t\right] \right\} \quad (1)$$
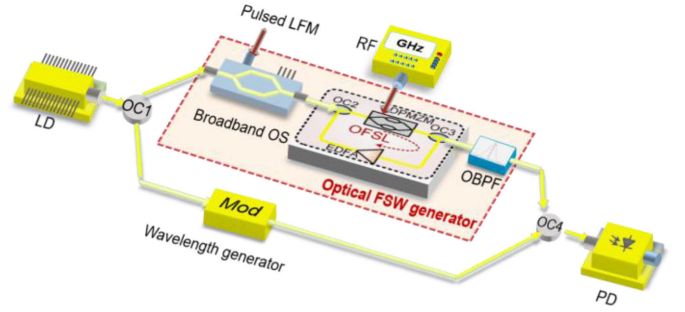

Fig. 1. Schematic diagram the proposed waveform generator. LD: laser diode; OS: optical switch; OC: optical coupler; OFSL: optical frequency shifting loop; DPMZM: dual-parallel Mach-Zehnder modulator; OBPF: optical bandpass filter; FSW: frequency-stepped waveform; PD: photodetector.

where ω_o is the angular frequency of the optical carrier, P is an integer, and $T_s = P\tau$. Eq. (1) is an expression of an optical FSW [27]. The frequency-stepping period and time duration of the optical FSW are τ and T_s, respectively. When the driven signal of the OS is changed to be an electrical rectangular LFM pulse with an expression given by,

$$s(t) = \sum_n rect\left[\frac{t-nT_s-\tau/2}{\tau}\right]$$
$$\times \cos\left[\omega_m(t-nT_s) + 2k(t-nT_s)^2\right] \quad (2)$$

where ω_m is the start angular frequency of electrical LFM signal, and $k = B/4\tau$, B is the bandwidth of the LFM signal, and an optical bandpass filter (OBPF) is employed to remove the unwanted components, the output of the OFSL would change to be,

$$E_{\mathrm{OFSL}}(t) = \sum_{n=0} \left\{ rect\left[\frac{t-nT_s-T_s/2}{T_s}\right] \cdot \sum_{p=0}^{P-1} rect\left[\frac{t-p\tau-nT_s-\tau/2}{\tau}\right] \right.$$
$$\left. \cdot \cos\left[(\omega_o + p\omega_s + \omega_m)(t-p\tau-nT_s) + 2k(t-p\tau-nT_s)^2\right] \right\} \quad (3)$$

When the LFM waveform has a bandwidth equaling ω_s, Eq. (3) can be rewritten as,

$$E_{\mathrm{OFSL}}(t) = \sum_{n=0} rect\left[\frac{t-nT_s-T_s/2}{T_s}\right]$$
$$\cdot \cos\left[(\omega_o + \omega_m)(t-nT_s) + \frac{PB}{2T_s}(t-nT_s)^2\right] \quad (4)$$

Eq. (4) represents an optical linearly-chirped waveform with a start frequency of $\omega_{o+}\omega_m$ and a bandwidth of PB.

The optical linearly-chirped waveform is then beating together with the wavelength output by the optical wavelength generator at a PD. When a single wavelength is produced by the optical wavelength generator, the electrical current output by the PD can be expressed as,

$$E_{\mathrm{PD}}(t) = \sum_{n=0} rect\left[\frac{t-nT_s-T_s/2}{T_s}\right]$$
$$\cdot \cos\left[\Delta\omega_1(t-nT_s) + \frac{PB}{2T_s}(t-nT_s)^2\right] \quad (5)$$

where $\Delta\omega_1$ is the detuning frequency between the optical wavelength from the optical wavelength generator and the start
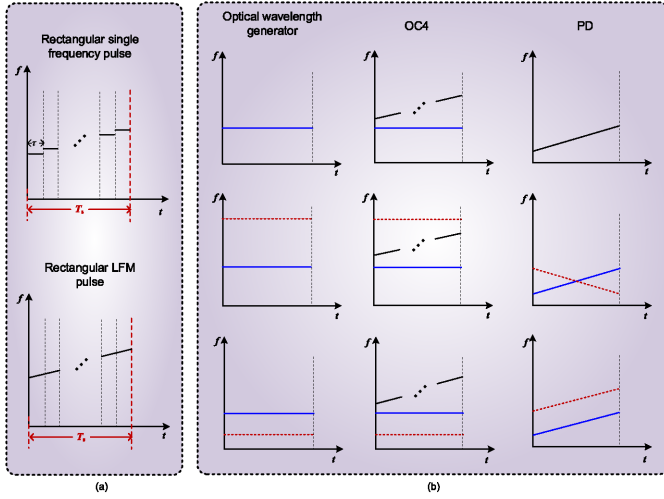
Fig. 2.   Illustration of instantaneous frequency curves of the optical and electrical signals at different locations. (a) at the output of the OFSL, (b) at the output of the optical wavelength generator, OC4, and PD.

Fig. 3.   The optical spectra of (a) the optical frequency-stepped signal and (b) the optical linear-chirped signal at the output of the OFSL.

frequency of the optical linear-chirped signal. As a result, an LFM signal is obtained with a start frequency of $\Delta\omega_1$ and a bandwidth of PB, as shown in the first line of Fig. 2(b).

When two wavelengths are produced by the optical wavelength generator, the electrical current at the output of the PD would become,

$$
\begin{aligned}
E_{\mathrm{PD}}\left(t\right) = & \sum_{n=0} rect\left[\frac{t-nT_{\mathrm{s}}-T_{\mathrm{s}}/2}{T_{\mathrm{s}}}\right] \\
& \cdot \left\{ \cos\left[\Delta\omega_2\left(t-nT_{\mathrm{s}}\right)+\frac{PB}{2T_{\mathrm{s}}}(t-nT_{\mathrm{s}})^2\right]\right. \\
& \left. + \cos\left[\Delta\omega_3\left(t-nT_{\mathrm{s}}\right)+\frac{PB}{2T_{\mathrm{s}}}(t-nT_{\mathrm{s}})^2\right]\right\}
\end{aligned}
\tag{6}
$$

where $\Delta\omega_2$ and $\Delta\omega_3$ are the detuning frequencies between the two optical wavelengths from the optical wavelength generator and the start frequency of the optical linear-chirped signal.

If the two optical wavelengths are located on the same side (i.e., both wavelengths larger or smaller) of the optical linear-chirped signal, Eq. (6) would be a dual-band LFM signal with the same linear-chirped slope, as illustrated in the third line of Fig. 2(b).

If the two optical wavelengths are located at different sides of the optical linear-chirped signal, Eq. (6) would be a counter-chirped LFM signal, as illustrated in the middle line of Fig. 2(b).

If more wavelengths are produced by the optical wavelength generator, LFM signals with multi-bands and multi-chirped frequencies can be generated. Therefore, a multi-functional LFM signal generator is realized.

III. EXPERIMENTS AND RESULTS

A proof-of-concept experiment based on the setup shown in Fig. 1 is carried out. An LD (TeraXion NLL04) is employed to produce a 1550.528-nm lightwave with a power of 14 dBm, which is then divided evenly into two branches. One of the branches is sent into an OS and the OFSL to generate an optical FSW, and the other one is sent to an optical wavelength generator. The OS is realized by an intensity modulator (IM,
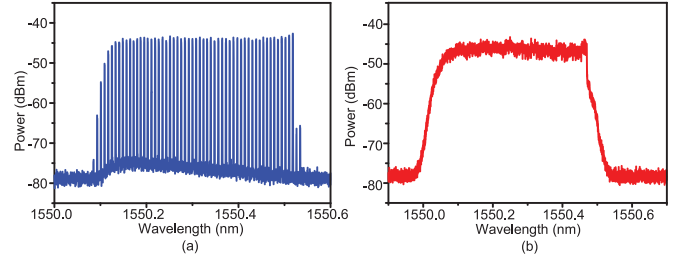
Fujitsu FTM7938EZ) driven by an electrical rectangular pulse. The OFSL is implemented by two OCs (OC2, OC3), a DP-MZM (Fujitsu FTM7961), and an amplifier with a loop length of ~42 m. The optical wavelength generator is achieved by another DPMZM (Fujitsu FTM7961). The 3-dB bandwidth and half-wave voltage of the IM are 25 GHz and 2.8 V, respectively, and those of the DPMZM are 22 GHz and 3.5 V, respectively. The two branches are then combined with an optical coupler (OC4) and beaten at a 30-GHz PD with a responsivity of 0.65 A/W.

When an electrical rectangular pulse is applied to the OS, an OFSW can be generated at the output of the OFSL with optical spectra shown in Fig. 3(a). The pulse width and period of the pulse are 208 ns and 12 μs, respectively. The OFSL is driven by a1-GHz RF signal. From Fig. 3(a) we can see that, about 50 optical combs with a frequency spacing of 1 GHz over a wavelength range from 1550.12 nm to 1550.52 nm are observed with a power fluctuation < 2 dB, indicating that, the generated OFSW has a flat power. The bandwidth is confined by an OBPF, without which, more frequency components can be obtained. Then the electrical rectangular pulse is switched to be a rectangular LFM pulse which is produced by an electrical waveform generator. The pulsed LFM signal has the same pulse width and period with the electrical rectangular pulse, and the LFM signal is from 7 to 8 GHz. The optical spectrum is then changed to be Fig. 3(b), from which we can see, a broadband optical signal with a wavelength from 1550.064 to 1550.464 nm is observed. The frequency gaps of Fig. 3(a) are filled with the LFM signal, and the central frequency can be shifted by changing the central frequency of the electrical driven LFM signal.

The signal is then combined with the output of the optical wavelength generator via OC4. The optical wavelength generator is realized by a DPMZM. Firstly, no RF signal is applied to the optical wavelength generator and the DPMZM is biased at the maximum transmission point (MATP). The output optical signal of OC4 is shown in Fig. 4(a), which is then converted into the electrical domain with the followed PD. The spectrum, waveform, instantaneous frequency, auto-correlation function and cross-correlation function of the generated signal are shown in Fig. 4(b), (c), (d), (e) and (f). The instantaneous frequency in Fig. 4(d) is obtained with short-time Fourier transform (STFT) function, from which we can see that a single-chirped LFM signal with frequency from 8 to 32 GHz is generated, corresponding to a 'P' of Eq. (4) as 24. The time duration is around 5 μs, corresponding to a TBWP of ~120000. The 3-dB pulse width
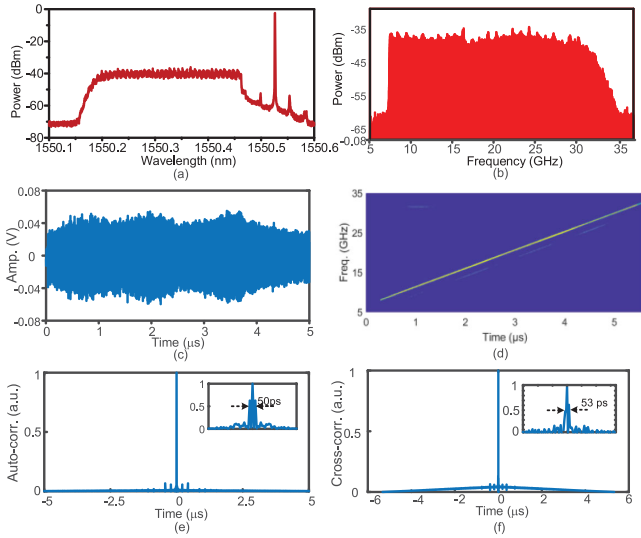
Fig. 4. (a) The optical spectrum, (b) the electrical spectrum, (c) the waveform, (d) the instaneous frequency curve, (e) the auto-correlation function and (f) the cross-correlation function of the generated single-chirped LFM signal.
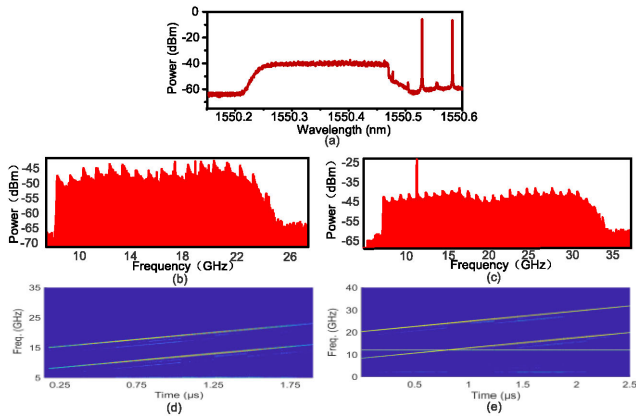

Fig. 5. (a) The optical spectrum, (b, c) the electrical spectra and (c, d) the instantaneous frequency curves of the dual-band LFM signals.

of the auto-correlated pulse is about 50 ps, resulting in a pulse compression ratio (PCR) of 100000. The relatively poor PCR mainly results from the imperfect harmonic suppression. The 3-dB pulse width of the cross-correlated pulse is about 37.5 ps, indicating that the two signals have a good phase correlativity.

When an RF signal is applied to the optical wavelength generator and the DPMZM is controlled to realize single-sideband modulation, there would be two optical wavelengths generated. Fig. 5(a) shows the output spectra of OC4 when the frequency of the RF signal is 7 GHz and the two wavelengths are placed at the same side of the optical LFM signal. An OBPF is inserted to confine the bandwidth of the optical LFM signal to be ~0.064 nm. Then the signal is beaten at a PD. Fig. 5(b), (d) shows the spectrum and the instantaneous frequency of the generated signal, indicating that, a dual-band LFM signal with a frequency of 8–16 GHz and 15–23 GHz over a time duration of ~1.6 μs is generated, corresponding to a 'P' of Eq. (4) as 8.
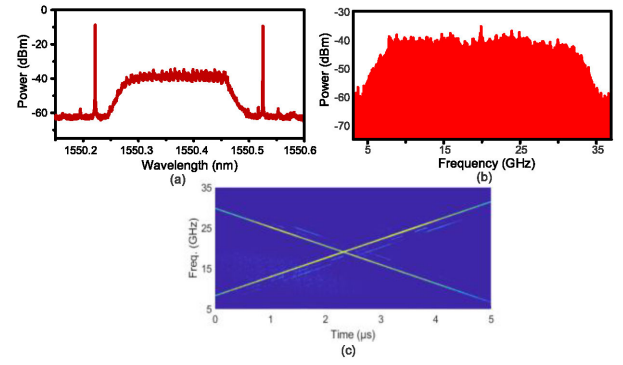

Fig. 6. (a) The optical spectrum and (b) the electrical spectrum and (c) the instantaneous frequency curve of the generated counter-chirped LFM signal.

The beaten signal between the two optical wavelengths (7-GHz signal) is removed with an electrical filter. It should be noted that the central frequency can be adjusted by changing the frequency of the RF signal and the bandwidth can be adjusted by controlling the OBPF. For example, when the frequency of the RF signal is increased to 12 GHz and the bandwidth of the OBPF is adjusted to ~0.096 nm, a dual-band LFM signal with a frequency of 8–20 GHz and 20–32 GHz over a time duration of ~2.5 μs is observed, as shown in Fig. 5(c), (e). However, there is a large 12-GHz signal, which is the beaten signal of the two optical wavelengths. The signal is hard to be removed with an electrical filter since it is overlapping with the generated dual-band signal. To remove the signal, microwave photonic co-site RF cancellation method [28] can be employed. In addition, since the LFM signal can be pulse-compressed, the effect of the single frequency may be rejected after auto-correlation.

Then the RF signal is tuned to be 20 GHz, and the DPMZM is biased at the MATP to remains only the even-order sidebands. As a result, two optical wavelengths placed at different sides of the optical LFM signal can be generated. Combined the optical wavelengths with the optical LFM signal and beaten them at a PD, a counter-chirped LFM signal is obtained. Fig. 6 displays the optical spectrum observed before PD, the spectrum and the instantaneous frequency curve of the generated counter-chirped LFM signal. From Fig. 6 we can see that, the counter-chirped waveform is from 8 to 32 GHz over a time duration of 5 μs, corresponding to a TBWP of 120000. The frequency and the bandwidth can also be tuned by adjusting the RF frequency and the OBPF. In addition, the maximum bandwidth can be further improved if the bandwidth of the PD is increased, and more formats of LFM signals can be obtained if more wavelengths are produced by the optical wavelength generator.

The ambiguity function of the obtained LFM waveforms is also analyzed to evaluate the range-Doppler resolution, which is calculated according to its expression [20]. Fig. 7(a), (b) and (c) display the ambiguity functions of the linear-chirped, dual-band and counter-chirped LFM waveforms, respectively, and Fig. 7(d), (e) and (f) are the according contour maps of the three functions. As can be seen, the ambiguity functions of the linear-chirped and dual-band LFM waveforms shown in Fig. 7(a) and (b) have similar shapes, i.e., the knife-edge shape,
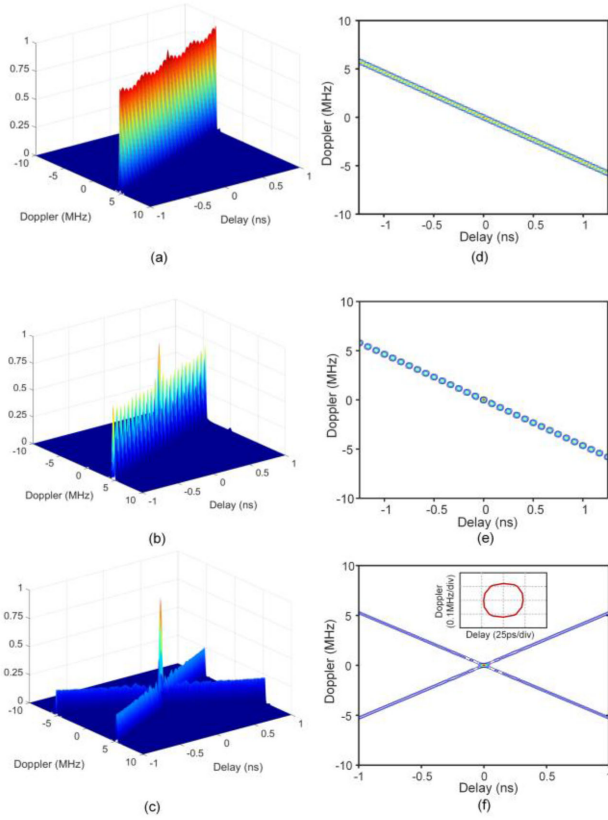
Fig. 7. The ambiguity functions and corresponding contour maps of the generated (a, d) linear-chirped, (b, e) dual-band and (c, f) counter-chirped LFM signals.
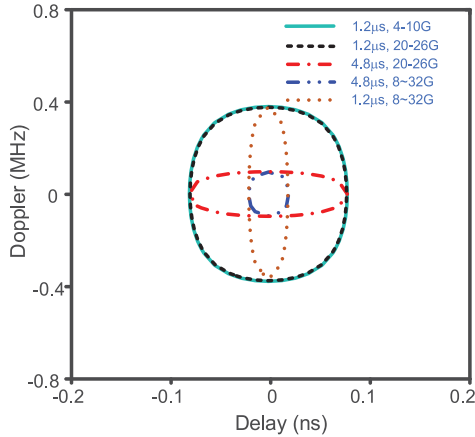

Fig. 8. Contour maps of the dual-LFM signals with different time durations and bandwidths.

while that of the counter-chirped LFM signal is a pushpin-shape ambiguity function. The 3-dB contour map of the ambiguity function of the counter-chirped LFM waveform is shown in the inset of Fig. 7(f), indicating that the counter-chirped signal has a good range-Doppler resolution. The resolution can be further increased if the time duration and the bandwidth of the obtained waveforms are increased.

Fig. 8 shows the simulated 3-dB contour maps of the ambiguity functions of counter-chirped LFM signals with different time durations, bandwidthes and central frequencies. From the black-half-dashed and the red dash-dotted curves we can conclude that, the doppler resolution is inversely proportional to the time duration, while from the red-dash-dotted and the blue-dash-dot-dotted curves we can conclude that, the range resolution is inversely proportional to the bandwidth. From the simulation results, we can draw conlusions that the range-Doppler resolution is related with the bandwidth and the time duration of the dual-chirpd LFM signals regardless of the central frequency, and the larger the time-bandwidth product of the counter-chirped LFM signal is, the smaller the area of the 3-dB contour map is. Actually, the proposed structure can easily be expanded to generate counter-chirped LFM signals with a large time-bandwidth product when a PD with a larger bandwidth is employed. As a result, a better range-doppler resolution can be achieved. However, limited by the observation range of the 32-GHz oscilloscope, extensions are not carried out.

IV. DISCUSSIONS

A. Impact of Power Imbalance on the Range-Doppler Resolution

Generally, a counter-chirped LFM signal can be expressed as [20],

$$i_{\rm d}(t) = \frac{1}{\sqrt{2}}\frac{1}{\sqrt{T}}rect\left(\frac{t}{T}\right)\left[e^{j\left(\Omega t+kt^2\right)}+e^{j\left(\Omega t-kt^2\right)}\right] \quad (7)$$

where T, Ω and k are the time duration, the central angular frequency, and the chirp rate of the linear-chirped waveform, respectively, and $k = B/2T$, where B is the waveform bandwidth. However, due to the uneven amplitude response of the optical waveform generator, the powers of the two chirped signals of the dual-chirp waveform are not the same. The expression can be rewritten as,

$$i_{\rm d}(t) = \frac{1}{\sqrt{1+a^2}}\frac{1}{\sqrt{T}}rect\left(\frac{t}{T}\right)\left[e^{j\left(\Omega t+kt^2\right)}+ae^{j\left(\Omega t-kt^2\right)}\right] \quad (8)$$

where a is the amplitude of the negative-chirped LFM signal that related to the positive-chirped LFM signal. The corresponding ambiguity function of the signal in (8) can be given by [20],

$$|\chi_s\left(\tau,\Omega_d\right)|^2 = \frac{1}{(1+a^2)^2}\left|\left(1-\frac{|\tau|}{T}\right)\frac{\sin\left[\frac{1}{2}T(2k\tau+\Omega_d)\left(1-\frac{|\tau|}{T}\right)\right]}{\frac{1}{2}T(2k\tau+\Omega_d)\left(1-\frac{|\tau|}{T}\right)}\right.$$
$$\left.+a^2\left(1-\frac{|\tau|}{T}\right)\frac{\sin\left[\frac{1}{2}T(\Omega_d-2k\tau)\left(1-\frac{|\tau|}{T}\right)\right]}{\frac{1}{2}T(\Omega_d-2k\tau)\left(1-\frac{|\tau|}{T}\right)}\right|^2 \quad (9)$$

Fig. 9 displays the simulated 3-dB contour maps of the ambiguity functions of dual-chired LFM signals with $a = 0.6$, 0.7, 0.8, 0.9, 1. As can be seen from Fig. 9, the area of the 3-dB contour map increases gradually when a changes from 1 to 0.6 with an interval of -0.1, indicating that the shape of the ambiguity function changes from pushpin shape to knife-edge shape gradually, and the range-Doppler resolution is worsen. Therefore, to achieve a better range-Doppler resolution, the two contrary-chirped LFM signals of the counter-chirped LFM
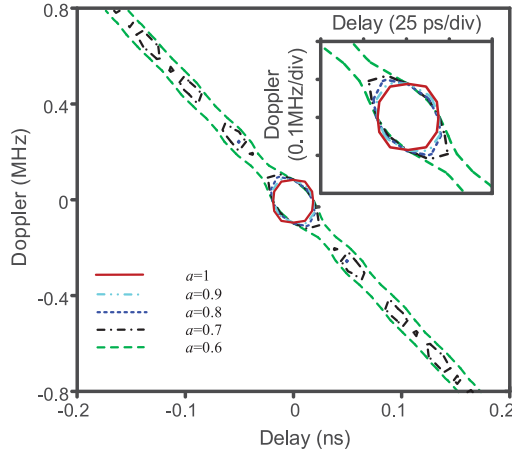
Fig. 9. Contour maps of the LFM signals with different time durations and bandwidths.

Fig. 10. 3-dB contour maps of the LFM signals with different time durations and bandwidths.

signal should have the same power, which can be realized by carefully adjusting the power of the two wavelengths that generated from the optical wavelength generator.

B. Impact of Single-Frequency Spur on the Range-Doppler Resolution

From Fig. 5 we can see that, there would be single-frequency spur remained with the generated LFM signa. In this section, we are exploring the impact of the single-frequency spur on the range-Doppler resolution. The expression of a counter-chirped LFM signal incorporated with a single frequency spur can be written as,

$$i_{\mathrm{ds}}(t) = \frac{1}{\sqrt{2+b^2}} \frac{1}{\sqrt{T}} rect\left(\frac{t}{T}\right) \left[e^{j\left(\Omega t + kt^2\right)} + e^{j\left(\Omega t - kt^2\right)} + be^{j(\Omega t)}\right] \quad (10)$$

where b is the amplitude of the single-frequency spur that related to the counter-chirped LFM signal. Then the corresponding ambiguity function can be calculated to be,

$$|\chi_s(\tau, \Omega_d)|^2 = \frac{1}{(2+b^2)^2} \left| \left(1 - \frac{|\tau|}{T}\right) \frac{\sin\left[\frac{1}{2}T(2k\tau + \Omega_d)\left(1 - \frac{|\tau|}{T}\right)\right]}{\frac{1}{2}T(2k\tau + \Omega_d)\left(1 - \frac{|\tau|}{T}\right)} \right.$$
$$+ \left(1 - \frac{|\tau|}{T}\right) \frac{\sin\left[\frac{1}{2}T(\Omega_d - 2k\tau)\left(1 - \frac{|\tau|}{T}\right)\right]}{\frac{1}{2}T(\Omega_d - 2k\tau)\left(1 - \frac{|\tau|}{T}\right)}$$
$$\left. + b^2\left(1 - \frac{|\tau|}{T}\right) \frac{\sin\left[\frac{1}{2}T\Omega_d\left(1 - \frac{|\tau|}{T}\right)\right]}{\frac{1}{2}T\Omega_d\left(1 - \frac{|\tau|}{T}\right)} \right|^2 \quad (11)$$

Fig. 10 shows the simulation results of the 3-dB contour maps of the ambiguity functions when $b = 0, 1, 2, 3$, respectively. As can be seen from Fig. 10, when $b = 1$, i.e., the single-frequency spur has the same amplitude with the counter-chirped LFM signal, the corresponding ambiguity function has the smallest contour map, indicating that under this condition, the signal has the best range-Doppler resolution. That is to say, in the proposed system, if a single-frequency signal is generated together with the counter-chirped LFM signal and it has the same amplitude
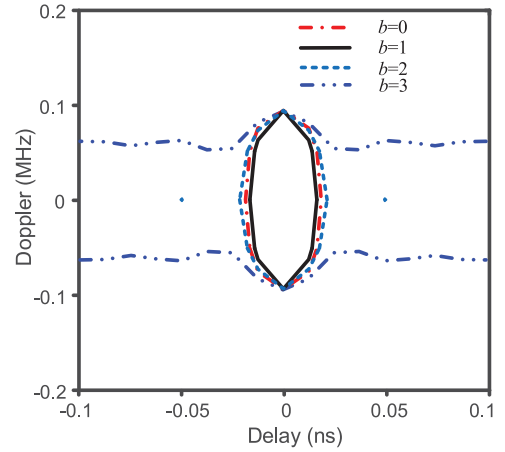
with the counter-chirped LFM signal, the range-Doppler resolution can be improved. Actually, from Fig. 6(a) we can see that, this kind of signal can be easily obtained if the bandwidth of the PD is broad enough.

V. CONCLUSION

In conclusion, a multi-functional and reconfigurable LFM waveform generator is proposed and experimentally demonstrated by using an OFSL and an optical wavelength generator. Single-chirped and counter-chirped waveforms of 8–32 GHz with a 5-μs time duration are obtained, and dual-band LFM waveforms of 8–16 GHz & 15–23 GHz with a 1.6-μs time duration and 8–20 GHz & 20–32 GHz with a 2.5-μs time duration are obtained. The ambiguity functions of the generated three kinds of LFM signals are evaluated, knife-edge-type ambiguity functions are obtained for single-chirped and dual-band LFM signals and pushpin-type ambiguity function is obtained for counter-chirped LFM signal, indicating that counter-chirped LFM signal has a good range-Doppler resolution. The impacts of the power imbalance of the counter-chirped LFM signal and the remained single-frequency spur on the range-Doppler resolution are analyzed, showing that a counter-chirped LFM signal with uniform amplitudes incorporated with a single-frequency signal that has the same amplitude with the counter-chirped signal has the best range-Doppler resolution. The proposed signal generator can be potentially scaled to multiple bands, which can be employed in multi-functional radar systems or MIMO radar systems to increase the range-resolution, the range-Doppler resolution and the flexibility of the systems.

REFERENCES

[1] M. Skolnik, in *Radar Handbook*, 3rd ed. NY, NY, USA: McGraw-Hill, 2008.
[2] J. Yao, "Arbitrary waveform generation," *Nat. Photon*, vol. 4, no. 2, pp. 79–80, 2010.
[3] S. L. Pan and Y. M. Zhang, "Microwave photonic radars," *IEEE J. Lightw. Technol*, vol. 38, no. 19, pp. 5450–5484, Oct. 2020.

[4] J. Capmany and D. Novak, "Microwave photonics combines two worlds," *Nat. Photon*, vol. 1, no. 6, pp. 319–330, 2007.

[5] J. Yao, "Microwave photonics," *IEEE/OSA J. Lightw. Technol.*, vol. 27, no. 3, pp. 314–335, 2009.

[6] S. Pan, D. Zhu, and F. Zhang, "Microwave photonics for modern radar systems," *Trans. Nanjing Univ. Aeronaut. Astronaut.*, vol. 31, no. 3, pp. 219–240, 2014.

[7] C. Wang and J. Yao, "Chirped microwave pulse generation based on optical spectral shaping and wavelength-to-time mapping using a sagnac loop mirror incorporating a chirped fiber bragg grating," *IEEE/OSA J. Lightw. Technol.*, vol. 27, no. 16, pp. 3336–3341, Aug. 2009.

[8] M. Li, L. Shao, J. Albert, and J. Yao, "Tilted fiber bragg grating for chirped microwave waveform generation," *IEEE Photon. Technol. Lett.*, vol. 23, no. 5, pp. 314–316, Mar. 2011.

[9] Y. Li, A. Rashidinejad, J. Wun, D. Leaird, J. Shi, and A. Weiner, "Photonic generation of W-band arbitrary waveforms with high time-bandwidth products enabling 3.9 mm range resolution," *Optica*, vol. 1, no. 6, pp. 446–454, 2014.

[10] A. Rashidinejad and A. Weiner, "Photonic radio-frequency arbitrary waveform generation with maximal time-bandwidth product capability," *J. Lightw. Technol.*, vol. 32, no. 20, pp. 3383–3393, 2014.

[11] Y. Zhang, X. Ye, Q. Guo, F. Zhang, and S. Pan, "Photonic generation of linear-frequency-modulated waveforms with improved time-bandwidth product based on polarization modulation," *IEEE/OSA J. Lightw. Technol.*, vol. 35, no. 10, pp. 1821–1829, May 2017.

[12] P. Zhou, F. Zhang, Q. Guo, and S. Pan, "Linearly chirped microwave waveform generation with large time-bandwidth product by optically injected semiconductor laser," *Opt. Express*, vol. 24, no. 16, pp. 18460–18467, 2016.

[13] P. Zhou, F. Zhang, Q. Guo, S. Li, and S. Pan, "Reconfigurable radar waveform generation based on an optically injected semiconductor laser," *IEEE J. Sel. Topics Quantum Electron.*, vol. 23, no. 6, 2017, Art. no. 1801109.

[14] F. Z. Zhang *et al.*, "Photonics-based broadband radar for high-resolution and real-time inverse synthetic aperture imaging," *Opt. Express*, vol. 25, no. 14, pp. 16274–16281, 2017.

[15] R. Li *et al.*, "Demonstration of a microwave photonic synthetic aperture radar based on photonic-assisted signal generation and stretch processing," *Opt. Express*, vol. 25, no. 13, pp. 14334–14340, 2017.

[16] A. Wang, J. Wo, X. Luo, Y. Wang, and W. Cong, "Ka-band microwave photonic ultra-wideband imaging radar for capturing quantitative target information," *Opt. Express*, vol. 26, no. 16, pp. 20708–20717, 2018.

[17] X. W. Ye, F. Z. Zhang, Y. Yang, and S. L. Pan, "Photonics-based radar with balanced I/Q de-chirping for interference-suppressed high-resolution detection and imaging," *Photon. Res.*, vol. 7, no. 3, pp. 265–272, 2019.

[18] L. E. Y. Herrera, R. M. Ribeiro, V. B. Jabulka, P. Tovar, and J. Weid, "Photonic generation and transmission of linearly chirped microwave pulses with high TBWP by self-heterodyne technique," *IEEE/OSA J. Lightw. Technol.*, vol. 36, no. 19, pp. 4408–4415, Oct. 2018.

[19] J. W. Shi *et al.*, "Photonic generation and wireless transmission of linearly/nonlinearly continuously tunable chirped millimeter-wave waveforms with high time-bandwidth product at W-band," *IEEE Photon. J.*, vol. 4, no. 1, pp. 215–223, Feb. 2012.

[20] D. Zhu and J. Yao, "Dual-chirp microwave waveform generation using a dual-parallel Mach-Zehnder modulator," *IEEE Photon. Technol. Lett.*, vol. 27, no. 13, pp. 1410–1413, Jul. 2015.

[21] Q. S. Guo, F. Z. Zhang, P. Zhou, and S. L. Pan, "Dual-band LFM signal generation by frequency quadrupling and polarization multiplexing," *IEEE Photon. Technol. Lett.*, vol. 29, no. 16, pp. 1320–1323, Aug. 2017.

[22] X. Li, S. Zhao, Z. Zhu, K. Qu, T. Lin, and D. Hu, "Photonic generation of frequency and bandwidth multiplying dual-chirp microwave waveform," *IEEE Photon. J.*, vol. 9, no. 3, pp. 1–14, Jun. 2017.

[23] K. Zhang, S. Zhao, X. Li, W. Jiang, and G. Wang, "Photonic approach to dual-band dual-chirp microwave waveform generation with multiplying central frequency and bandwidth," *Opt. Commun.*, vol. 437, pp. 17–26, 2019.

[24] P. Zhou, H. Chen, N. Q. Li, R. H. Zhang, and S. L. Pan, "Photonic generation of tunable dual-chirp microwave waveforms using a dual-beam optically injected semiconductor laser," *Opt. Lett.*, vol. 45, no. 6, pp. 1342–1345, 2020.

[25] W. J. Chen, D. Zhu, C. X. Xie, T. Zhou, X. Zhong, and S. L. Pan, "Photonics-based reconfigurable multi-band linearly frequency-modulated signal generation," *Opt. Express*, vol. 26, no. 25, pp. 32491–32499, 2018.

[26] K. W. Holman, "200-GHz 8-μs LFM optical waveform generation for high-resolution coherent imaging," in *Proc. 19th Coherent Laser Radar Conf.*, 2018, Art. no. Th7.

[27] Y. M. Zhang, C. Liu, K. L. Shao, Z. Y. Li, and S. L. Pan, "Multi-octave and reconfigurable frequency-stepped radar waveform generation based on an optical frequency shifting loop," *Opt. Lett.*, vol. 45, no. 7, pp. 2038–2041, 2020.

[28] Y. Xiang, G. Li, and S. Pan, "Ultrawideband optical cancellation of RF interference with phase change," *Opt. Express*, vol. 25, no. 18, pp. 21259–21264, 2017.